

Article

Real-Time Monitoring of H₂O₂ Sterilization on Individual *Bacillus atrophaeus* Spores by Optical Sensing with Trapping Raman Spectroscopy

Morten Bertz ¹, Denise Molinnus ², Michael J. Schöning ^{2,3,*}  and Takayuki Homma ^{1,4,*}

¹ Research Organization for Nano & Life Innovation, Waseda University, 513 Waseda-Tsurumakichou, Shinjuku-ku, Tokyo 162-0041, Japan; m.bertz@kurenai.waseda.jp

² Institute of Nano-, and Biotechnologies (INB), Aachen University of Applied Sciences, Campus Jülich, Heinrich-Mußmann-Str.1, 52428 Jülich, Germany; molinnus@fh-aachen.de

³ Institute of Biological Information Processing (IBI-3), Research Center Jülich GmbH, 52428 Jülich, Germany

⁴ Department of Applied Chemistry, Waseda University, 3-4-1 Okubo, Shinjuku-ku, Tokyo 169-8555, Japan

* Correspondence: schoening@fh-aachen.de (M.J.S.); t.homma@waseda.jp (T.H.);
Tel.: +49-241-6009-53215 (M.J.S.); +81-3-5286-3209 (T.H.)

Abstract: Hydrogen peroxide (H₂O₂), a strong oxidizer, is a commonly used sterilization agent employed during aseptic food processing and medical applications. To assess the sterilization efficiency with H₂O₂, bacterial spores are common microbial systems due to their remarkable robustness against a wide variety of decontamination strategies. Despite their widespread use, there is, however, only little information about the detailed time-resolved mechanism underlying the oxidative spore death by H₂O₂. In this work, we investigate chemical and morphological changes of individual *Bacillus atrophaeus* spores undergoing oxidative damage using optical sensing with trapping Raman microscopy in real-time. The time-resolved experiments reveal that spore death involves two distinct phases: (i) an initial phase dominated by the fast release of dipicolinic acid (DPA), a major spore biomarker, which indicates the rupture of the spore's core; and (ii) the oxidation of the remaining spore material resulting in the subsequent fragmentation of the spores' coat. Simultaneous observation of the spore morphology by optical microscopy corroborates these mechanisms. The dependence of the onset of DPA release and the time constant of spore fragmentation on H₂O₂ shows that the formation of reactive oxygen species from H₂O₂ is the rate-limiting factor of oxidative spore death.

Keywords: optical sensor setup; Raman spectroscopy; optical trapping; *Bacillus atrophaeus* spores; sterilization; DPA (dipicolinic acid)



Citation: Bertz, M.; Molinnus, D.; Schöning, M.J.; Homma, T. Real-Time Monitoring of H₂O₂ Sterilization on Individual *Bacillus atrophaeus* Spores by Optical Sensing with Trapping Raman Spectroscopy. *Chemosensors* **2023**, *11*, 445. <https://doi.org/10.3390/chemosensors11080445>

Academic Editor: Jose V. Ros-Lis

Received: 11 July 2023

Revised: 7 August 2023

Accepted: 7 August 2023

Published: 10 August 2023



Copyright: © 2023 by the authors. Licensee MDPI, Basel, Switzerland. This article is an open access article distributed under the terms and conditions of the Creative Commons Attribution (CC BY) license (<https://creativecommons.org/licenses/by/4.0/>).

1. Introduction

To evaluate the performance of sterilization processes during aseptic food processing, bacterial spores are commonly used due to their extraordinary hardness against a wide variety of methods, such as heat, radiation, or chemical agents, for example, H₂O₂ [1–3]. A number of factors are thought to contribute to the resilience of spores—spores have several coat layers that provide mechanical stability and impermeable membranes that protect the core [4–6]. In the core, which corresponds to the cell body of the live bacterium, most water has been replaced with dipicolinic acid (DPA) in a 1:1 complex with divalent ions, mostly Ca²⁺. The low water content is thought to protect spores from heat stress [5,7]. Furthermore, specific proteins (small, acid-soluble spore proteins [SASPs]) have been suggested to protect the spore's DNA from damage by radiation or oxidizing agents [5,8,9].

Using spores to assess sterilization procedures is an established system, and aseptic packaging using H₂O₂, either in the gas or liquid phase, is used on an industrial scale [2]; however, despite this widespread use, the actual mechanism of how H₂O₂ kills spores is surprisingly poorly understood [10]. H₂O₂ is a strong oxidizing agent, that decomposes

into reactive species, such as intermediates of hydroxyl/hydroperoxyl radicals, and this will ultimately result in the oxidation of the organic material that makes up the spore [11]. Early works have found that H_2O_2 treatment starts at the outside of the spore with damage to the coat resulting in lysis and finally dissolution [12,13]. Conversely, Ref. [14] suggested that H_2O_2 specifically damages the spore's inner membrane. At sublethal concentrations, the core remains intact but treated spores are sensitized to subsequent stress [14] or fail to grow after germination [15]. At higher concentrations, the weakening of this permeability barrier results in H_2O_2 influx and oxidative damage to proteins and DNA [4].

Recent studies have demonstrated that the sterilization process is accompanied by morphological changes of the spore upon H_2O_2 exposure [16,17]. Figure 1A,B show exemplary scanning electron microscopy (SEM) images of *Bacillus atrophaeus* spores before (A) and after (B) treatment with gaseous H_2O_2 . A clear difference between the treated and non-treated spores is visible with non-treated spores having a typical ellipsoid geometry with a diameter of about 500 nm and a length of 1–2 μm . In contrast, after sterilization, the spores are distinctly deformed or even completely collapsed due to the ruptured spore shell [17,18]. In addition, more detailed experiments revealed the spore appearance being directly influenced by the applied gaseous H_2O_2 concentration [16]. Three different categories were found: normal spores (without H_2O_2 exposure), deformed spores (below about 7% v/v H_2O_2), and flattened spores (above 7% v/v H_2O_2). The morphology changes also correlated with the spores' height changes from originally about 530 to about 240 nm. Both SEM and atomic force microscopy (AFM) studies gave comparable results. Interestingly, this behavior is observed for different types of spores, e.g., for *Bacillus atrophaeus*, *Bacillus subtilis*, and *Geobacillus stearothermophilus* [16].

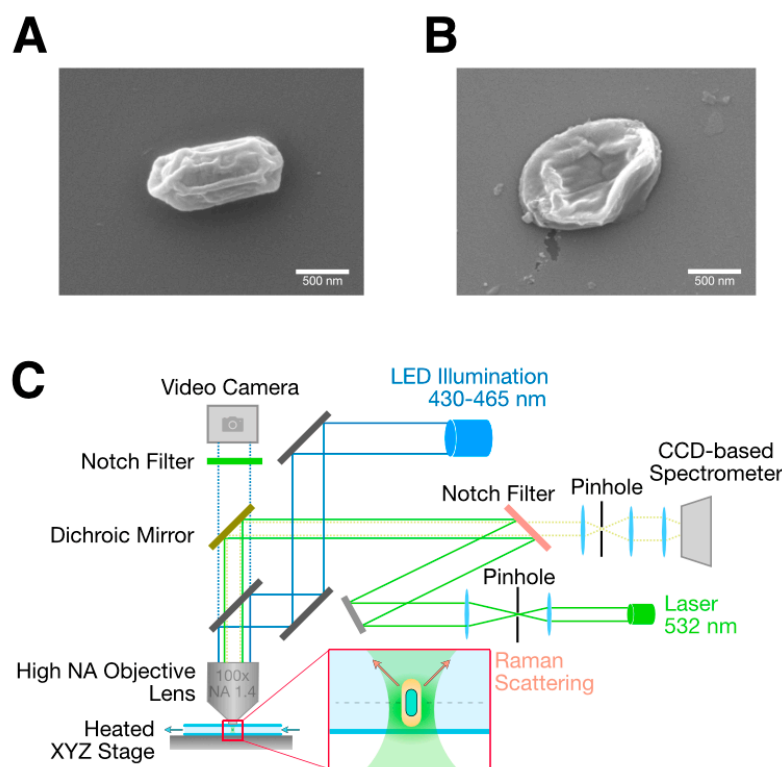


Figure 1. Scanning electron microscopy images of *Bacillus atrophaeus* spores before (A) and after (B) treatment with H_2O_2 . (C) Schematic of the confocal optical trapping Raman microscopy setup. Individual spores are trapped using a green 532 nm laser focused through a high NA objective lens. Raman scattering is collected through the same lens and analyzed using a CCD-based spectrometer. Bright-field imaging is performed using narrow-band blue light illumination and a video camera. NA: numerical aperture, CCD: charge-coupled device.

A number of sensor approaches have been proposed in the literature to monitor spore viability and/or spore damage by H_2O_2 in the gas or liquid phase. Examples include (Bio) chemical sensors detecting biomarkers such as mRNA (messenger ribonucleic acid), DPA, or Ca^{2+} ions [19,20], piezoelectric sensors with immobilized antibodies specific to *Bacillus anthracis* spores [21,22], and potentiometric chemosensors based on a surface-imprinted polymer for the selective determination of DPA [23,24]. In addition, impedimetric sensors, for example, DNA aptamer-based viability sensors for the detection of *S. typhimurium* bacteria [25], or a reusable, universal impedimetric sensor based on a bacteria-imprinted polythiophene film have made the rapid and sensitive detection of pathogenic bacteria possible [26]. However, all these methods suffer from the fact that they have response times of at least several to tens of minutes (which precludes real-time validation of spore degradation), or are incompatible with in situ experiments, i.e., gaseous conditions.

In recent work, changes in spore morphology due to gaseous H_2O_2 sterilization were characterized by means of a novel impedimetric spore-based biosensor [16,17]. The sensor chip consisted of an IDE (interdigitated electrode)-based differential set-up with an active element carrying immobilized spores and a reference element without spores. Changes in the differential impedance signal (active to passive IDE) with varying H_2O_2 concentrations correlate with the spores' morphology changes. This way, the impedance change reflects sporicidal efficacy. In addition, the dosed H_2O_2 concentration of aseptic filling machines can be monitored by a calorimetric gas sensor utilizing MnO_2 as a catalytically active material to guarantee operational functionality [27,28]. Even though the above-discussed sensor method addresses the qualitative and quantitative validation of spore degradation, this technique cannot reveal the "short-term" mechanism of spore rupture in situ in the time frame of a few seconds or less, and thus essentially only provides "before" and "after" snapshots.

On the other hand, optical sensing based on Raman spectroscopy has found widespread use as it provides non-destructive label-free chemical information that can be used to detect and classify biological organisms. Consequently, Raman spectroscopy has been employed for species-specific spore detection and to assess inactivation procedures [29]. The combination of Raman spectroscopy with an optical trap permits the isolation of individual, micron-sized particles from suspension and thus permits continuous, long-term observation of single bacteria or cells [30,31]. Here, a tightly focused laser beam generates an attractive force sufficient to trap and hold micron-sized objects at the focus of the beam [32] in solution. Optical trapping Raman spectroscopy (OTRS) has been used to investigate the effect of oxidative damage on individual yeast cells [33] and human retinal pigment epithelium cells [34]. The germination of *Bacillus thuringiensis* spores has been followed by monitoring the DPA biomarker [35] and Zhang et al. [36] have used OTRS to observe the wet-heat inactivation dynamics of single *Bacillus* spores to indicate that treatment at >80 °C leads to protein denaturation followed by the release of DPA from the spore.

In this work, we focus for the first time on the mechanism underlying oxidative damage of *Bacillus atrophaeus* by H_2O_2 which is commonly used in sterilization processes. Following a spore's chemical composition in situ by means of an optical sensing technique such as OTRS should ideally directly uncover this mechanism. In principle, oxidative damage could occur primarily at the inner membrane resulting in lysis. On the other hand, damage could commence from the spore's outer coat, stripping away layer by layer until the spore is dissolved. In our experiment, individual trapped spores are observed at high temporal resolution to discern the chemical changes occurring during oxidative damage. Simultaneous bright field microscopy follows changes in the spore's morphology and refractivity during this process. Investigating oxidative damage at different concentrations of H_2O_2 , the combination of these optical sensing techniques provides a detailed understanding of the process of H_2O_2 sterilization on the molecular level.

2. Materials and Methods

2.1. Sample Preparation

Bacillus atrophaeus spores (ATCC 9372, lot BT258) were obtained from Crosstex, Englewood, CO, USA. Sample suspensions were prepared by diluting 20 μL of the spore stock suspension (nominal population 2.4×10^6 spores per 100 μL) with 1000 μL of deionized water followed by 4 cycles of centrifugation (16,000 rpm for 2 min) and resuspension to remove contaminants and residual ethanol of the stock suspension. After preparation, the concentration of the spore suspension was adjusted to have, on average, fewer than one spore per 600 $\mu\text{m} \times 600 \mu\text{m}$ field of view in the sample chamber to avoid accidental trapping of two spores during an experiment. Spore suspensions were freshly prepared daily before the Raman experiments. Atmospheric oxygen was removed from all sample solutions by bubbling with nitrogen.

2.2. Raman Microscope Setup

The optical trapping Raman microscope (see Figure 1C) was based on a Nanofinder 30 confocal Raman microscope (Tokyo Instruments, Tokyo, Japan). The optical trap was formed by focusing a green 532 nm laser through a 100 \times magnification oil immersion lens (UPlanSApo, NA 1.4, Olympus, Tokyo, Japan). Raman-scattered light was collected using the same objective lens and analyzed using an EMCCD (Electron-Multiplied Charge-Coupled Device)-based spectrometer (Andor Newton DU970P_BV) cooled to $-70 \text{ }^\circ\text{C}$ equipped with a 600 grooves/mm grating. Simultaneous bright-field imaging was conducted by illuminating the sample with a narrowband LED (laser-emitting diode, 430–465 nm, X-Cite XLED1) in a spectral range that minimizes interference with the Raman measurements. A notch filter placed in front of the EMCCD camera (Andor iXon) was used to remove elastically scattered laser light from the acquired images. The spring constant of the optical trap was estimated using the equipartition theorem method [37] by analyzing the positional variance of a trapped 1 μm polystyrene particle from video images.

2.3. Raman Spectroscopy and Data Analysis

Sample chambers were constructed from coverslips and separated by $\approx 120 \mu\text{m}$ spacers (total volume $\approx 30 \mu\text{L}$). After injecting the spore suspension, the chamber was sealed with vacuum grease and mounted in the microscope. Individual spores were visually identified by bright-field microscopy and trapped in the laser beam. Spectra were acquired between 900 and 3200 cm^{-1} at a spectral resolution of $\approx 1.5 \text{ cm}^{-1}$ in 8 s intervals. The laser power was 2 mW at the exit pupil of the objective lens. Bright-field images were acquired using an EMCCD camera (Andor Ixon) at 6 frames per second with an exposure time of 10 ms. The sample was only illuminated during exposures. For measurements in the presence of H_2O_2 , the spore suspension was mixed with the appropriate amount of H_2O_2 from a 35% stock solution (Fujifilm Wako Pure Chemicals, Osaka, Japan) to a final concentration from 0.2–5% v/v H_2O_2 , injected into the sample chamber, mounted, and analyzed.

Data were analyzed using custom-written software in Igor Pro 8.0 (Wavemetrics, Portland, OR, USA). Intensity profiles of selected Raman peaks were computed by a running sum between the edges of each peak of interest and subtracting the linear baseline that connects the two edges. As the trapped spore was held in a stable focus position by the optical trap, no spectral normalization was required to extract intensity profiles from the time scans of individual spores. The start of all timed courses were defined as the spore entering the trap, as judged from the bright-field video. Bright-field intensity profiles were obtained by calculating the average intensity of the spore image. Spore tracking was performed by fitting a two-dimensional Gaussian function to each spore image. Time courses were fit with sigmoidal or single-exponential functions.

2.4. Scanning Electron Microscopy

For studying the surface morphology and geometry of the spores (*Bacillus atrophaeus*) before and after the sterilization process, a scanning electron microscope (JSM-7800F,

JEOL Ltd., Akishima City, Japan) was utilized. For imaging, each spore sample was additionally coated by sputtering with a 10 nm Pt/Pd (80:20) conductive layer.

3. Results and Discussion

Our optical trapping setup is based on a conventional confocal Raman microscope (see Figure 1C). Simultaneous optical trapping Raman spectroscopy and bright-field imaging give access to the trapped spore's chemical composition and appearance. Using the same laser for trapping and spectroscopy also provides a robust autofocusing mechanism that keeps the observed spore at the focus of the laser beam throughout the experiment. The spring constant of the trap is around 7 pN/ μm , which permits the detection of Brownian motion of the trapped spore (see Supplementary Video S1).

Figure 2 contains Raman spectra (left diagram) and brightfield images (right) of a single trapped spore at various points in time, i.e., after 50, 250, 310, and 710 s, respectively (an additional video containing Raman spectra and video imaging of the entire trapping experiment is provided as Supplementary Video S1). The spore enters the trapping laser at the center of the brightfield images at $t = 0$ s after undergoing random Brownian motion throughout the field of view. The concentration of spores in the sample chamber was adjusted to avoid a second spore accidentally entering the trap by Brownian motion for the duration of an experiment (≈ 10 – 15 min, see Section 2 for details). As soon as the spore enters the trap, the long axis of the cylindrical spore body orients itself along the propagation direction of the laser beam adopting the geometry illustrated in the inset in Figure 1C. From this point in time, Raman spectra were collected to investigate the spore's chemical makeup at a temporal resolution of 8 s/spectrum. Since the focal volume of the confocal Raman microscope is of similar dimensions as the spore's cell body ($\approx 1 \mu\text{m}^3$), the spectra reflect the average chemical composition of the entire spore.

A typical spectrum of the trapped spore obtained 50 s after trapping is shown in the black bottom trace in Figure 2 (left). This spectrum is dominated by different peaks stemming from DPA, a key component of the spore's core, which is indicated in teal at 1017 cm^{-1} , 1399 cm^{-1} , 1447 cm^{-1} , and 1573 cm^{-1} [38]. The peak at 1017 cm^{-1} provides a readily detectable fingerprint of DPA and has been widely used to investigate the DPA concentration in spores [35,38]. In addition, we can also discern peaks reflecting the protein content (marked red in Figure 2) of the spore via the amide I vibration (1657 cm^{-1}), phenylalanine ring breathing (1004 cm^{-1}), and vibrations of aromatic side chains (1604 cm^{-1}), but these bands occur at lower intensity compared to DPA and are thus partially obscured [29]. $\text{CH}_{2/3}$ -stretching at 2941 cm^{-1} originates from methyl/methylene groups in a variety of biological molecules, e.g., proteins, lipids, or carbohydrates, and can thus be considered a proxy for the total amount of organic material present in the spore. Table 1 contains a detailed assignment of the vibrational bands found in *B. atrophaeus* during a trapping experiment to their respective chemical entities.

The spectra of the trapped spore remained unchanged for about 200 s after trapping. During this time, there were no changes in the relative amounts of DPA and organic content after the spore had settled in a trap, as shown in the time courses in Figure 3A. Here, the teal and violet traces represent the DPA and organic content, respectively, in a single trapped spore over time. After 250 s of trapping, however, the spore's Raman spectra started to evolve (blue spectrum in Figure 2). Most prominently, peaks originating from DPA started disappearing, indicating a leakage of DPA. This manifests itself as a sharp drop in the DPA content in the time course in Figure 3A. DPA release concludes within ≈ 60 s, as can be seen in the green spectrum recorded 310 s after the spore has entered the trap (60 s after the onset of DPA release) in Figure 2, where the DPA peaks have now entirely vanished. DPA release is accompanied by a loss of organic material (Figure 3A, violet trace) which commences at the same time but follows a much slower, more gradual time course.

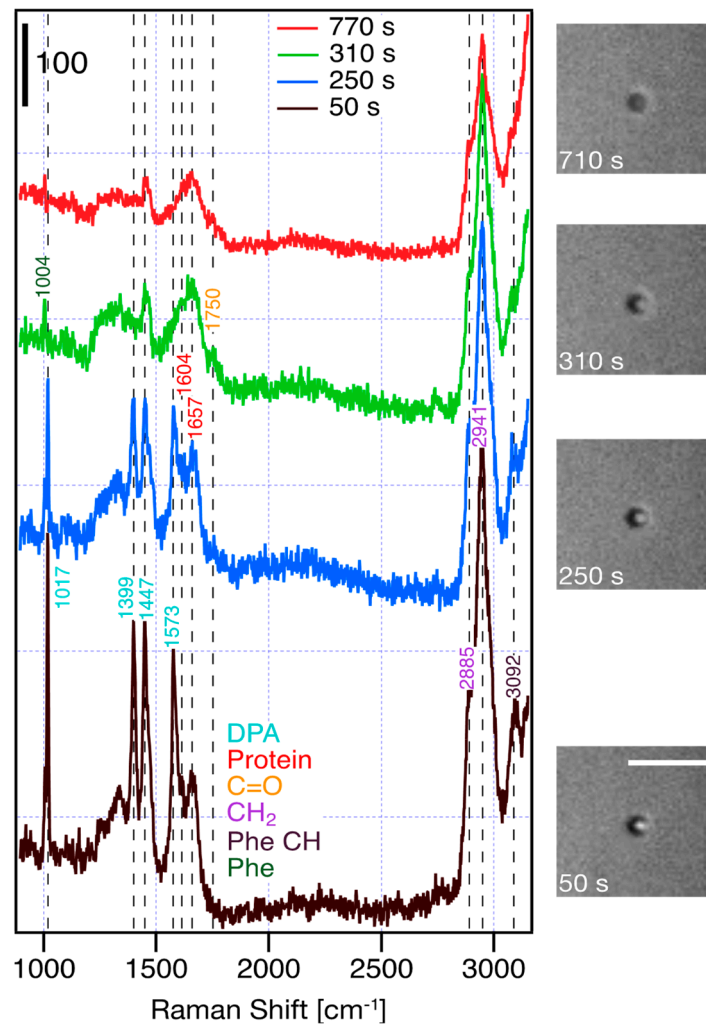


Figure 2. Raman spectra of a single trapped spore of *Bacillus atrophaeus* 50 s, 250 s, 310 s, and 710 s after entering the trap (left, from bottom to top). Characteristic peaks and their chemical assignment are indicated in the figure (left, DPA: dipicolinic acid, Phe: phenylalanine ring breathing). Bright-field images of the trapped spore at various points in time (right, from bottom to top, 50 s, 250 s, 310 s, 710 s). The scale bar is 5 μm .

Table 1. Assignment of Raman bands in spectra of individual *B. atrophaeus* spores to their chemical entities.

Raman Shift [cm^{-1}]	Assignment
1004	Phe (ring breathing)
1017	DPA ring breathing
1399	DPA COO ⁻ stretch (symmetric)
1447	DPA C-C ring stretch
1573	DPA COO ⁻ stretch (asymmetric)
1604	Protein (Tyr, Trp, Phe)
1657	amide I
1750	C=O
2885	CH ₂
2941	CH ₂
3092	Phenyl CH

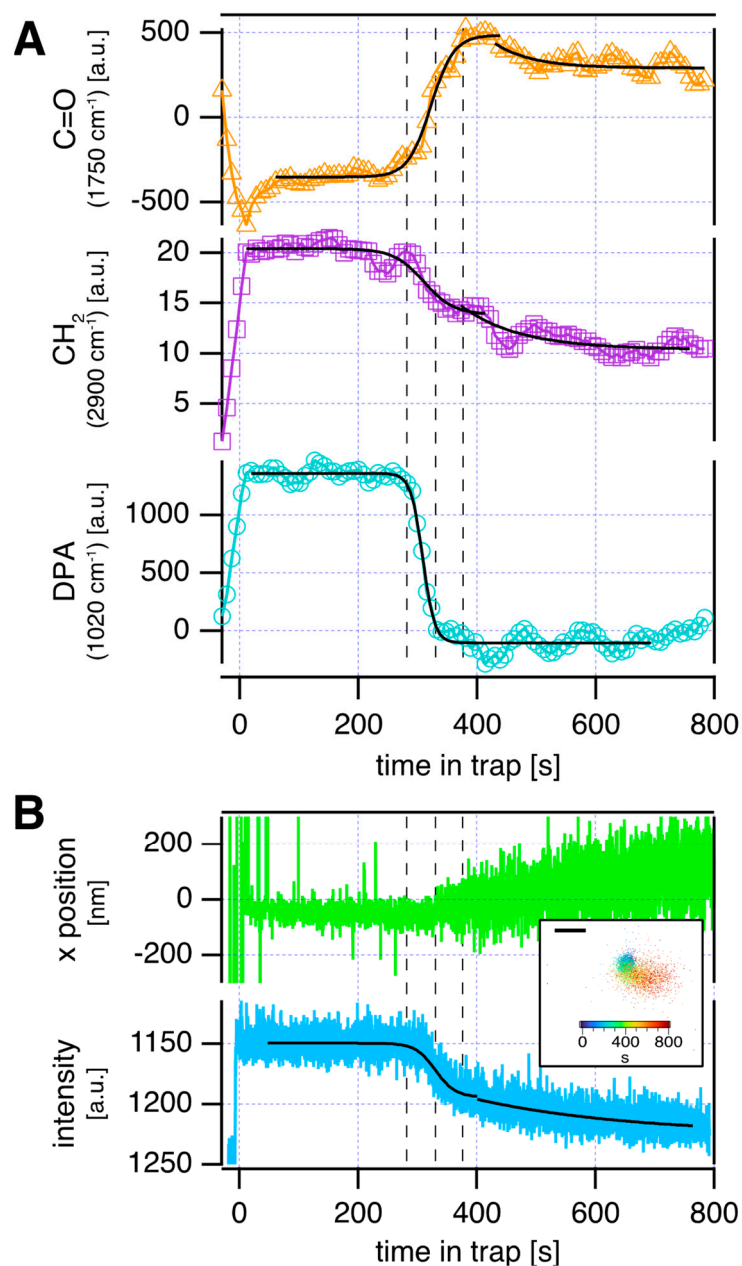


Figure 3. Changes of morphology and composition of a single spore during trapping. **(A)** From bottom to top: Time courses of the Raman signals representing dipicolinic acid (1017 cm^{-1} , teal), total organic content (2941 cm^{-1} , dark violet), and oxidation products (1750 cm^{-1} , orange). **(B)** The intensity of the spore's bright-field image (blue) and horizontal displacement of the spore from the center of the optical trap (green), were obtained using simultaneous video microscopy. The inset shows the 2D position of the trapped spore throughout the experiment (scale bar 200 nm).

In addition, we can detect the emerging signature of the carbonyl vibrations at 1750 cm^{-1} (indicated in orange in Figure 2) after the point of DPA release, which indicates the formation of oxidation products in the spore. Interestingly, no oxidation products could be identified before the onset of DPA release. The formation of oxidation products proceeds on a timescale that parallels the loss of organic material and reaches a maximum of $\approx 120\text{ s}$ after DPA release (Figure 3A, orange).

While DPA leakage is complete after 310 s (Figure 3A, teal), organic material continues to be released from the spore following a slow exponential decay with a time constant of several hundred seconds (Figure 3A, violet). The amount of detected carbonyl compounds

(oxidation products) mirrors this overall loss of material: After the initial rapid increase between 250 and 380 s, oxidation appears complete and reaches a maximum, with a subsequent gradual drop in the amount of oxidized material on a timescale comparable to the loss of organic material (Figure 3A, orange). At the end of the experiment ($t = 770$ s, red spectrum in Figure 2), the intensity of proteinaceous content as well as overall organic material has dropped to about half of its original value at $t = 50$ s, with about half of this decrease occurring concurrently with DPA release and the remainder ensuing subsequently.

Bright-field imaging also gives us access to the spore morphology and appearance (see Supplementary Video S1). Snapshots of brightfield images of the spore corresponding to the Raman spectra in Figure 2 are shown in the right column of this figure. The bright circle at the center of the images reflects the trapped spore viewed along the long axis of its cylindrical body. While the limited spatial resolution of optical microscopy cannot provide detailed information on the morphology of the spore, it is evident that the loss in DPA between 50 s and 250 s coincides with a decrease in spore contrast. The spore's image at 250 s appears smaller and darker and this change continues after DPA has been released from the spore up until the very end of the experiment (710 s). We quantified this loss in contrast by plotting the average intensity in a 25×25 pixel region immediately surrounding the spore against time (Figure 3B, blue trace, and see Supplementary Video S2 for details).

The initial drop coincides with the release of DPA, with the subsequent decrease reflecting the loss of material upon oxidative damage of the spore shell. The timescale of the loss of brightfield intensity nicely mirrors the reduction of organic material in the spore (see Figure 3A center), indicating that these changes reflect the same underlying process. The release of DPA decreases the refractive index of the spore's core, which results in a loss of contrast as the refractive index approaches that of the surrounding aqueous medium [39,40]. Furthermore, we can also track the spore in the XY plane to analyze the diffusive motion of the spore in the harmonic trap potential (Figure 4B, green trace, and see Supplementary Video S2 for details). Fluctuations increase only upon the completion of DPA release which indicates a decrease in particle size at this stage of degradation.

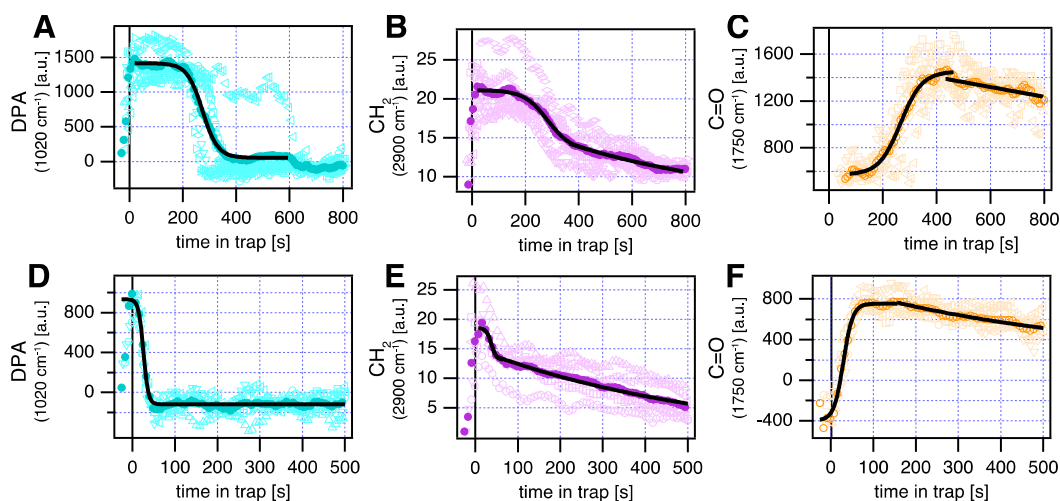


Figure 4. Optical trapping in the presence of H_2O_2 . The time course of the Raman signals representing dipicolinic acid (teal, left), total organic content (violet, center), and oxidation products (orange, right) in the absence (top, (A–C), $n = 5$) and presence (bottom, (D–F), $n = 5$) of 0.2% H_2O_2 . Averaged traces are indicated by closed symbols. The black lines represent fits to sigmoidal or single exponential functions.

In summary, there are three major changes in the spectra of trapped spores: loss of DPA, formation of oxidation products, and reduction of the organic content. The time evolution of these changes (Figure 3A) reveals a distinct sequence of steps during oxidative

damage. The initial step involves the rapid loss of DPA (Figure 3A bottom) accompanied by a general loss of spore material (Figure 3A center). Around the same time, oxidation products begin to form (Figure 3A top) and oxidation continues after lysis. This leads to a slow dissolution of the remaining shell, which can be seen as a loss of contrast and an overall decrease of spore content (Figure 3B), presumably into low molecular weight compounds that can diffuse away.

Figure 4A–C displays the Raman signals representing DPA, organic content, and oxidation products for several ($n = 5$) trapped spores. The initial step of spore degradation, i.e., the release of DPA, varies between 230 and 315 s (Figure 4A, light blue open symbols) with a mean value of 273 s (midpoint of DPA release, Figure 4A, dark blue filled symbols), and a similar scatter can be observed for the subsequent steps of oxidation and loss of organic material. Averaging over several spores (filled symbols in Figure 4A–C) blurs the transitions and makes the exact sequence of steps harder to discern compared to the single spore data presented in Figure 3. Nevertheless, all investigated spores in Figure 4A–C exhibited the same mechanism of degradation: DPA release followed by oxidation and loss of further material. This illustrates the advantages of the single-particle optical trapping assay compared to bulk experiments, which inherently suffer from a lack of synchronization between spores when performing experiments at the population level. Furthermore, single-particle experiments give access to the heterogeneity in spore lifetimes, which is crucial to assess the efficacy of sterilization processes [2] since individual, long-lived spores might be masked by the population average. The importance of spore-to-spore variability has long been recognized as important to quantify microbiological risk assessment [35,39,41], particularly in the light of super-dormant spores [6].

It might be surprising that spectral changes during trapping occur even in the absence of H_2O_2 (Figure 4A–C). Intense light can result in the production of reactive oxygen species from dissolved oxygen, either through direct absorption, resulting in singlet oxygen (1O_2), or through absorption by secondary molecules followed by photosensitization [42]. The latter process, which dominates when using light of a wavelength above 500 nm, results in the formation of reactive oxygen species (ROS), particularly superoxide ($\bullet O_2$). Correspondingly, superoxide can turn into hydrogen peroxide (H_2O_2) by reduction or dismutation, which can convert into the hydroxyl radical ($HO\bullet$) [43]. Naturally, ROS formation depends on the concentration of oxygen in the sample solution. During all trapping experiments, dissolved oxygen was minimized by purging all sample solutions with nitrogen to minimize ROS formation [44]. Omitting this step increases the amount of dissolved oxygen, which greatly reduces the spore lifetime under otherwise identical conditions (see Supplementary Figure S1). Mechanistically, light-induced spore death by reactive oxygen species is very similar to the action of H_2O_2 on the spore. The optical trapping assay hence mimics the action of H_2O_2 by illumination with green light. Moreover, ROS generated in situ via optical trapping have been successfully employed to investigate oxidative stress and signaling [45,46].

The addition of a low amount (0.2%) of H_2O_2 to the sample yields the same sequence of events (Figure 4D–F), albeit the lifetime of the spore is significantly reduced and the subsequent steps—formation of oxidation products and shell dissolution—are accelerated as well. At 0% H_2O_2 , DPA release takes ≈ 150 s until completion, which is reduced to 28 s upon the addition of 0.2% H_2O_2 (Figure 4A,D). The duration of oxidation is reduced from 100 s to 65 s, respectively (Figure 4C,F). This comes as no surprise as ROS generated from residual oxygen will react with H_2O_2 and trigger a chain reaction of H_2O_2 decomposition involving the production of further ROS (hydroxyl/hydroperoxyl radicals) as an intermediate species [47].

To study the H_2O_2 influence in more detail, Figure 5A displays the H_2O_2 concentration dependence of spore lifetime, which is defined as the midpoint of the sigmoidal DPA-release curves (black trace in Figure 4A,D). The full dataset contained in Figure 5 is presented in the Supplementary Figures S2 and S3. The addition of very low amounts (0.2%) of H_2O_2 reduced spore lifetime by an order of magnitude compared to pure water from 273 s to

26 s, respectively. At 2% H_2O_2 , the lifetime is reduced to 11 s and drops to 7 s at 5%. The sharp decrease in lifetime resulting from H_2O_2 addition reflects the increased amounts of reactive oxygen species produced from H_2O_2 by the illumination with green light. The concentration dependence of spore lifetime on the H_2O_2 concentration is, however, comparatively mild, with a doubling of concentration leading to a $\approx 50\%$ reduction in lifetime. This suggests that the spore lifetime is ultimately determined by the concentration of ROS. In our experiment, the amount of ROS depends not only on the H_2O_2 concentration but also on other factors, among them the incident laser power, or the amount of residual oxygen dissolved in the sample solutions. While this makes a comparison with industrial sterilization processes that rely on heat, light (i.e., UV light), or heavy metals (iron or copper) to trigger the formation of ROS difficult [48], extrapolating our data to the industrially relevant concentration of about 7–8% H_2O_2 [28] would result in a lifetime of less than 2 s.

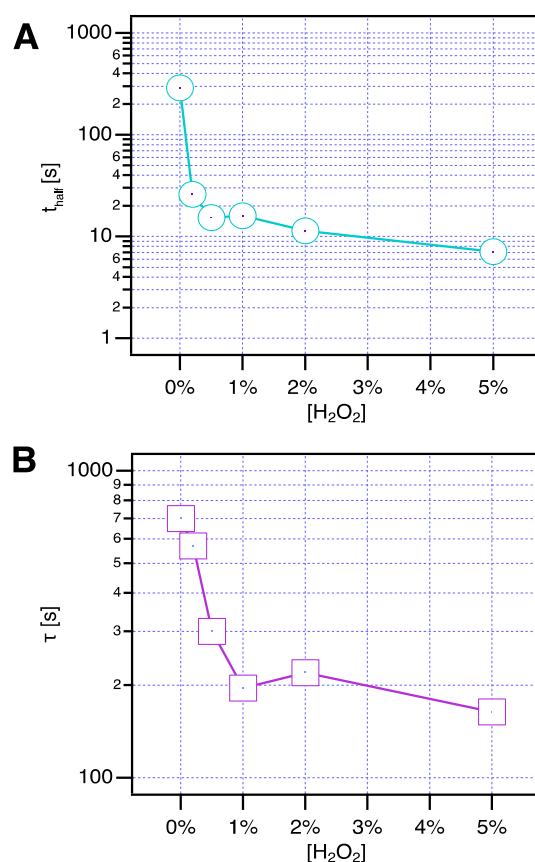


Figure 5. H_2O_2 concentration dependence of spore lifetime. (A) The time between spore trapping and DPA release and (B) time constant of spore dissolution as a function of H_2O_2 concentration (see also Supplementary Information, Figure S3).

Spore dissolution (Figure 5B) is characterized by the release of organic material, which proceeds via a slow, exponential decrease that occurs after the initial drop of organic content simultaneous to DPA release due to inner membrane rupture (Figure 4B,E). This loss of organic material likely involves the fragmentation of macromolecules, such as proteins, lipids, and carbohydrates, into smaller compounds by the oxidative action of H_2O_2 . These fragments can then dissociate from the spore and diffuse away. The time constant of the dissolution process (Figure 5B) follows an approximately exponential relationship with respect to the H_2O_2 concentration with an initially strong decrease between 0% and 1% H_2O_2 followed by an almost constant plateau region between 1% and 5%. This indicates that between 0% and 1%, oxidation and dissolution still occur simultaneously for a significant amount of time, which slows down the loss of organic material. At higher concentrations of

H_2O_2 beyond 1%, oxidation is essentially complete after the release of DPA so the plateau of the time constant of around 200 s reflects the speed limit of low-molecular-weight oxidation products detaching from the remaining spore shell.

The amount of remaining organic material at the end of the dissolution process is similar for all concentrations of H_2O_2 studied (Supplementary Figure S3 right column), which suggests that the remaining spore shell consists of highly oxidized and/or oxidation-resistant organic material. It is important to note that oxidation of proteins can lead to both fragmentation (via cleavage of peptide bonds) or crosslinking of proteins or protein fragments [48], which prevents the complete disintegration of the spore.

Taken together, we arrive at the following model of oxidative spore death by H_2O_2 (Figure 6): H_2O_2 decomposition, triggered by catalysts, heat, or light, results in damage to the inner membrane surrounding the spore core (Figure 6, panel 2). The weakening of this permeability barrier leads to the rapid outflux of DPA, and the influx of ROS into the core (Figure 6, panel 3), resulting in the formation of oxidation products via the reaction with the remaining organic material (Figure 6, panel 4). This ultimately leads to the partial dissolution of the remaining spore shell (Figure 6, panel 5) leaving behind remnants of the cortex and coat (Figure 6, panel 6, and Figure 1B). The inner membrane has long been identified as the target of oxidative action [4]. Low, sublethal oxidative treatment sensitizes the spores to subsequent stress by inner membrane damage and prevents the successful outgrowth of survivors [14,15]. In contrast, we find that under conditions of high oxidative stress, the inner membrane ruptures resulting in the rapid loss of DPA akin to the effect of wet heat on spores [36]. The duration of DPA release by oxidative damage is faster compared to DPA release during germination [35], suggesting wide-ranging damage to the inner membrane.

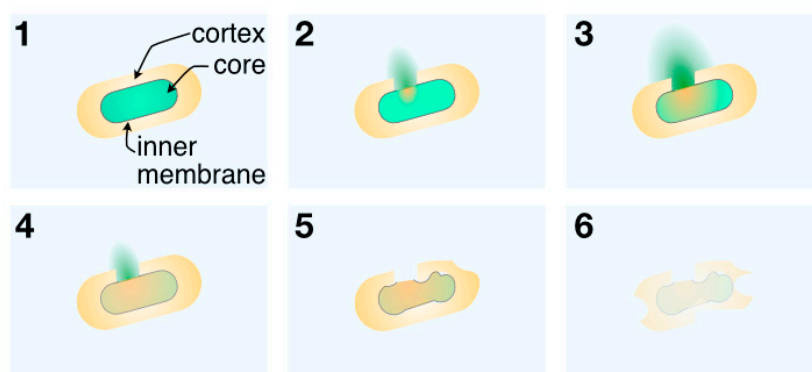


Figure 6. Model of the sporicidal action of H_2O_2 : Original spore without H_2O_2 treatment (1). Breach of the inner membrane (2) leads to DPA release (3) and the formation of oxidation products (4). The remaining spore shell (5), then gradually dissolves (6) in a H_2O_2 concentration-dependent manner.

This is further supported by the observation that the duration of DPA release becomes shorter with H_2O_2 concentration (Figure 4A,D) since higher amounts of H_2O_2 are expected to result in more and faster damage to the inner membrane. Rapid DPA loss has also been directly observed upon treatment with the oxidizing sterilization agent peracetic acid (PAA) [49] or upon laser irradiation [50] in the related organism *B. thuringiensis*. Interestingly, oxidation products only start to form after the breach of the inner membrane, which allows the influx of ROS into the core (Figure 3A). This indicates that no significant oxidation of the spore cortex and coat is taking place even in the presence of high amounts of oxidizing agent (5% H_2O_2). The presence of detoxifying enzymes in the outer layers of the spore, i.e., catalase to destroy H_2O_2 and superoxide dismutase to eliminate superoxide, have been implicated in spore resistance to oxidative damage [5]. Moreover, weakening of the inner membrane in the presence of oxidizing agents has been suggested to primarily proceed via the disruption of sulphhydryl and disulfide bonds of proteins rather than through the direct oxidation of amino acids [51]. Only after the inner membrane has been breached

oxidation of organic compounds in the core can take place. The resulting fragmentation of macromolecules leads to a loss of organic material, leaving behind an empty spore shell as seen in Figure 1B. Similar changes to spore appearance resulting from H₂O₂ treatment as well as their H₂O₂ concentration dependence have been previously detected by SEM and AFM [16] while fragmentation of the spore coat was observed by high-resolution transmission electron microscopy after PAA treatment [49]. On the other hand, all these techniques are rather bulky and do not allow in situ analysis, which is possible by our optical sensor setup with Raman scattering (loss of organic material), optical microscopy (loss of refractivity), and particle tracking (decrease in size). The proposed single-spore assay directly reveals the intricate sequence of steps of spore degradation during treatment with oxidizing agents such as hydrogen peroxide.

4. Conclusions

A mechanistic understanding of how spores are killed by sterilization agents is important to evaluate and optimize the efficacy of sterilization processes. Despite their widespread use, the influence of oxidative sterilization agents such as gaseous H₂O₂ on the spores' lifetime and inactivation has not yet been studied by in situ sensor methods in detail. Here, we used optical trapping Raman spectroscopy (OTRS) to follow the fate of an individual spore under conditions of high oxidative stress. Exposure to reactive oxygen species (ROS) resulted in a breach of the inner membrane and the release of DPA after a lag time, which became shorter with an increase in H₂O₂ concentration. DPA loss could be directly detected spectroscopically and also manifested itself as a loss of spore refractivity, which we observed simultaneously with Raman measurements. Inner membrane rupture permits H₂O₂ influx into the core and triggers the oxidation of the remaining core content, e.g., proteins and DNA. Finally, additional material is lost from the spore shell through fragmentation of the residual material. The formation of ROS represents the rate-limiting step of the sterilization reaction, which in our experiment occurs through a combination of H₂O₂ exposure and illumination with visible light. This reproduces some aspects of industrial sterilization processes, such as H₂O₂ treatment and the combination of H₂O₂ with light illumination to facilitate ROS generation, but leaves out other factors, for example, elevated temperatures. To fully assess spore degradation under conditions mimicking those in aseptic filling machines, separating the formation of ROS by light from ROS formation originating from the sterilization agent itself (e.g., by thermal decomposition) would be desirable. Therefore, for future experiments, the optical sensor setup might be performed using near-infrared light at low intensities, which should minimize light-induced ROS generation [52]. Such an experiment would provide full control over the amount of ROS generated, for example, by controlling the temperature. Being an optical sensor method, OTRS is, in addition, highly robust against the harsh conditions required to kill spores, which would enlarge its applicability for a wide variety of sterilization processes.

Supplementary Materials: The following supporting information can be downloaded at: <https://www.mdpi.com/article/10.3390/chemosensors11080445/s1>, Video S1: Time-lapse of the optical trapping experiment; Figure S1: Dependence of trapped spore lifetime on ambient oxygen; Video S2: Changes of spore size and morphology during oxidative degradation; Figure S2: H₂O₂ concentration dependence of spore lifetime; Figure S3: Individual datasets of the H₂O₂ concentration dependence of spore lifetime.

Author Contributions: Conceptualization, M.B. and M.J.S.; investigation, M.B. and D.M.; writing—original draft preparation, M.B., D.M. and M.J.S.; writing—review and editing, M.B., D.M., M.J.S. and T.H.; supervision, M.J.S. and T.H.; funding acquisition, T.H. All authors have read and agreed to the published version of the manuscript.

Funding: This work was supported by the JST A-STEP program Development of Surface-Enhanced Raman Microscope with Plasmon Sensor for Ultra-Sensitive Surface and Interface Analysis (JP-MJTR202K, <https://doi.org/10.52926/JPMJTR202K>, accessed on 6 August 2023).

Institutional Review Board Statement: Not applicable.

Informed Consent Statement: Not applicable.

Data Availability Statement: The data presented in this study are available on request from the corresponding author.

Acknowledgments: The authors thank D. Rolka for the SEM measurements.

Conflicts of Interest: The authors declare no conflict of interest.

References

1. Ansari, I.A.; Datta, A.K. An overview of sterilization Methods for Packaging Materials Used in Aseptic Packaging Systems. *Food Bioprod. Process.* **2003**, *81*, 57–65. [[CrossRef](#)]
2. Jildeh, Z.B.; Wagner, P.H.; Schöning, M.J. Sterilization of objects, products, and packaging surfaces and their characterization in different fields of industry: The status in 2020. *Phys. Status Solidi A* **2021**, *218*, 2000732. [[CrossRef](#)]
3. Johnston, M.D.; Lawson, S.; Otter, J.A. Evaluation of hydrogen peroxide vapour as a method for the decontamination of surfaces contaminated with *Clostridium botulinum* spores. *J. Microbiol. Methods* **2005**, *60*, 403–411. [[CrossRef](#)]
4. Setlow, P. Spores of *Bacillus subtilis*: Their resistance to and killing by radiation, heat and chemicals. *J. Appl. Microbiol.* **2006**, *101*, 514–525. [[CrossRef](#)]
5. Setlow, P. Spore Resistance Properties. *Microbiol. Spectr.* **2014**, *2*, 615–622. [[CrossRef](#)]
6. Setlow, P.; Christie, G. What's new and notable in bacterial spore killing. *World J. Microbiol. Biotechnol.* **2021**, *37*, 144. [[CrossRef](#)] [[PubMed](#)]
7. Cho, W.I.; Chung, M.S. Bacillus spores: A review of their properties and inactivation processing technologies. *Food. Sci. Biotechnol.* **2020**, *29*, 1447–1461. [[CrossRef](#)]
8. Setlow, B.; Setlow, P. Binding of small, acid-soluble spore proteins to DNA plays a significant role in the resistance of *Bacillus subtilis* spores to hydrogen peroxide. *Appl. Environ. Microbiol.* **1993**, *59*, 3418–3423. [[CrossRef](#)]
9. Djouiaï, B.; Thwaite, J.E.; Laws, T.R.; Commichau, F.M.; Setlow, B.; Setlow, P.; Moeller, R. Role of DNA Repair and Protective Components in *Bacillus subtilis* Spore Resistance to Inactivation by 400-nm-Wavelength Blue Light. *Appl. Environ. Microbiol.* **2018**, *84*, e01604-18. [[CrossRef](#)]
10. Linley, E.; Denyer, S.P.; McDonnell, G.; Simons, C.; Maillard, J.Y. Use of hydrogen peroxide as a biocide: New consideration of its mechanisms of biocidal action. *J. Antimicrob. Chemother.* **2012**, *67*, 1589–1596. [[CrossRef](#)] [[PubMed](#)]
11. McDonnell, G. Peroxygens and other forms of oxygen: Their use for effective cleaning, disinfection, and sterilization. In *New Biocides Development. The Combined Approach of Chemistry and Microbiology*; Zhu, P.C., Ed.; American Chemical Society: Washington, DC, USA, 2007; pp. 292–308.
12. King, W.L.; Gould, G.W. Lysis of bacterial spores with hydrogen peroxide. *J. Appl. Bacteriol.* **1969**, *32*, 481–490. [[CrossRef](#)] [[PubMed](#)]
13. Shin, S.Y.; Calvisi, E.G.; Beaman, T.C.; Pankratz, H.S.; Gerhardt, P.; Marquis, R.E. Microscopic and thermal characterization of hydrogen peroxide killing and lysis of spores and protection by transition metal ions, chelators, and antioxidants. *Appl. Environ. Microbiol.* **1994**, *60*, 3192–3197. [[CrossRef](#)] [[PubMed](#)]
14. Cortezzo, D.E.; Koziol-Dube, K.; Setlow, B.; Setlow, P. Treatment with oxidizing agents damages the inner membrane of spores of *Bacillus subtilis* and sensitizes spores to subsequent stress. *J. Appl. Microbiol.* **2004**, *97*, 838–852. [[CrossRef](#)]
15. Setlow, B.; Yu, J.; Li, Y.Q.; Setlow, P. Analysis of the germination kinetics of individual *Bacillus subtilis* spores treated with hydrogen peroxide or sodium hypochlorite. *Lett. Appl. Microbiol.* **2013**, *57*, 259–265. [[CrossRef](#)]
16. Arreola, J.; Keusgen, M.; Wagner, T.; Schöning, M.J. Combined calorimetric gas- and spore-based biosensor array for online monitoring and sterility assurance of gaseous hydrogen peroxide in aseptic filling machines. *Biosens. Bioelectron.* **2019**, *143*, 111628. [[CrossRef](#)]
17. Oberländer, J.; Mayer, M.; Greeff, A.; Keusgen, M.; Schöning, M.J. Spore-based biosensor to monitor the microbicidal efficacy of gaseous hydrogen peroxide sterilization processes. *Biosens. Bioelectron.* **2018**, *104*, 87–94. [[CrossRef](#)]
18. Deng, X.; Shi, J.; Kong, M.G. Physical Mechanisms of Inactivation of *Bacillus subtilis* Spores Using Cold Atmospheric Plasmas. *IEEE Trans. Plasma Sci.* **2006**, *34*, 1310–1316. [[CrossRef](#)]
19. Baeumner, A.J.; Jones, C.; Wong, C.Y.; Price, A. A generic sandwich-type biosensor with nanomolar detection limits. *Anal. Bioanal. Chem.* **2004**, *378*, 1587–1593. [[CrossRef](#)]
20. Tehri, N.; Kumar, N.; Raghu, H.V.; Vashishth, A. Biomarkers of bacterial spore germination. *Ann. Microbiol.* **2018**, *68*, 513–523. [[CrossRef](#)]
21. Campbell, G.A.; Mutharasan, R. Piezoelectric-excited millimeter-sized cantilever (PEMC) sensors detect *Bacillus anthracis* at 300spores/mL. *Biosens. Bioelectron.* **2006**, *21*, 1684–1692. [[CrossRef](#)]
22. Wang, D.B.; Cui, M.M.; Li, M.; Zhang, X.E. Biosensors for the Detection of *Bacillus anthracis*. *Acc. Chem. Res.* **2021**, *54*, 4451–4461. [[CrossRef](#)]
23. Zhou, Y.; Yu, B.; Levon, K. Potentiometric sensor for dipicolinic acid. *Biosens. Bioelectron.* **2005**, *20*, 1851–1855. [[CrossRef](#)] [[PubMed](#)]

24. Orbay, S.; Kocaturk, O.; Sanyal, R.; Sanyal, A. Molecularly Imprinted Polymer-Coated Inorganic Nanoparticles: Fabrication and Biomedical Applications. *Micromachines* **2022**, *13*, 1464. [[CrossRef](#)]
25. Labib, M.; Zamay, A.S.; Kolovskaya, O.S.; Reshetneva, I.T.; Zamay, G.S.; Kibbee, R.J.; Sattar, S.A.; Zamay, T.N.; Berezovski, M.V. Aptamer-based viability impedimetric sensor for bacteria. *Anal. Chem.* **2012**, *84*, 8966–8969. [[CrossRef](#)] [[PubMed](#)]
26. Wang, L.; Lin, X.; Liu, T.; Zhang, Z.; Kong, J.; Yu, H.; Yan, J.; Luan, D.; Zhao, Y.; Bian, X. Reusable and universal impedimetric sensing platform for the rapid and sensitive detection of pathogenic bacteria based on bacteria-imprinted polythiophene film. *Analyst* **2022**, *147*, 4433–4441. [[CrossRef](#)]
27. Kirchner, P.; Li, B.; Spelthahn, H.; Henkel, H.; Schneider, A.; Friedrich, P.; Kolstad, J.; Keusgen, M.; Schöning, M.J. Thin-film calorimetric H₂O₂ gas sensor for the validation of germicidal effectivity in aseptic filling processes. *Sens. Actuators B Chem.* **2011**, *154*, 257–263. [[CrossRef](#)]
28. Kirchner, P.; Oberländer, J.; Friedrich, P.; Berger, J.; Rysstad, G.; Keusgen, M.; Schöning, M.J. Realisation of a calorimetric gas sensor on polyimide foil for applications in aseptic food industry. *Sens. Actuators B Chem.* **2012**, *170*, 60–66. [[CrossRef](#)]
29. Stöckel, S.; Schumacher, W.; Meisel, S.; Elschner, M.; Rösch, P.; Popp, J. Raman spectroscopy-compatible inactivation method for pathogenic endospores. *Appl. Environ. Microbiol.* **2010**, *76*, 2895–2907. [[CrossRef](#)]
30. Chan, J.W. Recent advances in laser tweezers Raman spectroscopy (LTRS) for label-free analysis of single cells. *J. Biophotonics* **2013**, *6*, 36–48. [[CrossRef](#)]
31. Redding, B.; Schwab, M.; Pan, Y.L. Raman Spectroscopy of Optically Trapped Single Biological Micro-Particles. *Sensors* **2015**, *15*, 19021–19046. [[CrossRef](#)] [[PubMed](#)]
32. Svoboda, K.; Block, S.M. Optical trapping of metallic Rayleigh particles. *Opt. Lett.* **1994**, *19*, 930–932. [[CrossRef](#)]
33. Chang, W.-T.; Lin, H.-L.; Chen, H.-C.; Wu, Y.-M.; Chen, W.-J.; Lee, Y.-T.; Liau, I. Real-time molecular assessment on oxidative injury of single cells using Raman spectroscopy. *J. Raman Spectrosc.* **2009**, *40*, 1194–1199. [[CrossRef](#)]
34. Chen, Y.; Wang, Z.; Huang, Y.; Feng, S.; Zheng, Z.; Liu, X.; Liu, M. Label-free detection of hydrogen peroxide-induced oxidative stress in human retinal pigment epithelium cells via laser tweezers Raman spectroscopy. *Biomed. Opt. Express.* **2019**, *10*, 500–513. [[CrossRef](#)] [[PubMed](#)]
35. Chen, D.; Huang, S.S.; Li, Y.Q. Real-time detection of kinetic germination and heterogeneity of single Bacillus spores by laser tweezers Raman spectroscopy. *Anal. Chem.* **2006**, *78*, 6936–6941. [[CrossRef](#)] [[PubMed](#)]
36. Zhang, P.; Kong, L.; Wang, G.; Setlow, P.; Li, Y.Q. Monitoring the wet-heat inactivation dynamics of single spores of Bacillus species by using Raman tweezers, differential interference contrast microscopy, and nucleic acid dye fluorescence microscopy. *Appl. Environ. Microbiol.* **2011**, *77*, 4754–4769. [[CrossRef](#)]
37. Sarshar, M.; Wong, W.T.; Anvari, B. Comparative study of methods to calibrate the stiffness of a single-beam gradient-force optical tweezers over various laser trapping powers. *J. Biomed. Opt.* **2014**, *19*, 115001. [[CrossRef](#)]
38. Huang, S.S.; Chen, D.; Pelczar, P.L.; Vepachedu, V.R.; Setlow, P.; Li, Y.Q. Levels of Ca²⁺-dipicolinic acid in individual bacillus spores determined using microfluidic Raman tweezers. *J. Bacteriol.* **2007**, *189*, 4681–4687. [[CrossRef](#)]
39. Hashimoto, T.; Friebe, W.R.; Conti, S.F. Germination of single bacterial spores. *J. Bacteriol.* **1969**, *98*, 1011–1020. [[CrossRef](#)] [[PubMed](#)]
40. Zhang, P.; Kong, L.; Wang, G.; Setlow, P.; Li, Y.-Q. Combination of Raman tweezers and quantitative differential interference contrast microscopy for measurement of dynamics and heterogeneity during the germination of individual bacterial spores. *J. Biomed. Opt.* **2010**, *15*, 056010. [[CrossRef](#)]
41. Stringer, S.C.; Webb, M.D.; George, S.M.; Pin, C.; Peck, M.W. Heterogeneity of times required for germination and outgrowth from single spores of nonproteolytic Clostridium botulinum. *Appl. Environ. Microbiol.* **2005**, *71*, 4998–5003. [[CrossRef](#)]
42. Blázquez-Castro, A. Optical Tweezers: Phototoxicity and Thermal Stress in Cells and Biomolecules. *Micromachines* **2019**, *10*, 507. [[CrossRef](#)] [[PubMed](#)]
43. Pryor, W.A.; Houk, K.N.; Foote, C.S.; Fukuto, J.M.; Ignarro, L.J.; Squadrito, G.L.; Davies, K.J. Free radical biology and medicine: It's a gas, man. *Am. J. Physiol. Regul. Integr. Comp. Physiol.* **2006**, *291*, R491–R511. [[CrossRef](#)] [[PubMed](#)]
44. Neuman, K.C.; Chadd, E.H.; Liou, G.F.; Bergman, K.; Block, S.M. Characterization of photodamage to Escherichia coli in optical traps. *Biophys. J.* **1999**, *77*, 2856–2863. [[CrossRef](#)]
45. Westberg, M.; Bregnhøj, M.; Blázquez-Castro, A.; Breitenbach, T.; Etzerodt, M.; Ogilby, P.R. Control of singlet oxygen production in experiments performed on single mammalian cells. *J. Photochem. Photobiol. A* **2016**, *321*, 297–308. [[CrossRef](#)]
46. Blázquez-Castro, A.; Westberg, M.; Bregnhøj, M.; Breitenbach, T.; Mogensen, D.J.; Etzerodt, M.; Ogilby, P.R. Light-initiated oxidative stress. In *Oxidative Stress*; Sies, H., Ed.; Academic Press: Cambridge, MA, USA, 2020; pp. 363–388. [[CrossRef](#)]
47. Oberländer, J.; Kirchner, P.; Boyen, H.-G.; Schöning, M.J. Detection of hydrogen peroxide vapor by use of manganese(IV) oxide as catalyst for calorimetric gas sensors. *Phys. Status Solidi A* **2014**, *211*, 1372–1376. [[CrossRef](#)]
48. McDonnell, G. The Use of Hydrogen Peroxide for Disinfection and Sterilization Applications. In *PATAI'S Chemistry of Functional Groups*; Rappoport, Z., Ed.; John Wiley & Sons, Ltd.: Chichester, UK, 2014; pp. 1–34. [[CrossRef](#)]
49. Malyshev, D.; Dahlberg, T.; Wiklund, K.; Andersson, P.O.; Henriksson, S.; Andersson, M. Mode of Action of Disinfection Chemicals on the Bacterial Spore Structure and Their Raman Spectra. *Anal. Chem.* **2021**, *93*, 3146–3153. [[CrossRef](#)]
50. Malyshev, D.; Öberg, R.; Dahlberg, T.; Wiklund, K.; Landström, L.; Andersson, P.O.; Andersson, M. Laser induced degradation of bacterial spores during micro-Raman spectroscopy. *Spectrochim. Acta A Mol. Biomol. Spectrosc.* **2022**, *265*, 120381. [[CrossRef](#)]

51. McDonnell, G.; Russell, A.D. Antiseptics and disinfectants: Activity, action, and resistance. *Clin. Microbiol. Rev.* **1999**, *12*, 147–179. [[CrossRef](#)]
52. Malyshev, D.; Robinson, N.F.; Öberg, R.; Dahlberg, T.; Andersson, M. Reactive oxygen species generated by infrared laser light in optical tweezers inhibits the germination of bacterial spores. *J. Biophotonics* **2022**, *15*, 118668. [[CrossRef](#)]

Disclaimer/Publisher’s Note: The statements, opinions and data contained in all publications are solely those of the individual author(s) and contributor(s) and not of MDPI and/or the editor(s). MDPI and/or the editor(s) disclaim responsibility for any injury to people or property resulting from any ideas, methods, instructions or products referred to in the content.